ELSEVIER

J. Non-Newtonian Fluid Mech. 96 (2001) 459–471

Journal of Non-Newtonian Fluid Mechanics

www.elsevier.com/locate/jnnfm

Wall effects for motion of spheres in power-law fluids

K.A. Missirlis [a], D. Assimacopoulos [a], E. Mitsoulis [b,*], R.P. Chhabra [c]

[a] *Department of Chemical Engineering, National Technical University of Athens, Athens 157-80, Greece*
[b] *Department of Mining Engineering and Metallurgy, National Technical University of Athens, Athens 157-80, Greece*
[c] *Department of Chemical Engineering, Indian Institute of Technology, Kanpur 208-016, India*

Received 13 March 2000; received in revised form 25 September 2000

Abstract

The steady motion of spheres representing particles inside tubes filled with different fluids has been investigated using both a finite-element and a finite-volume method. The rheology of the fluids has been modelled by the power-law able to describe the shear-thinning (pseudoplastic) behaviour of a series of polymer solutions. New results have been obtained for a series of tube/sphere diameter ratios in order to investigate the wall effects on the drag exerted by the fluid on the sphere. The results agree well with previous simulations for an unbounded medium (infinite diameter ratio). Experimental investigations have also been carried out and simulated, and the results compare favourably with the experiments. The present simulations revealed the convergence of the drag coefficient to a constant value independent of tube-to-sphere diameter ratio when the power-law index approaches zero.

Keywords: Power-law model; Finite-volume method; Non-orthogonal grid; Flow around a sphere; Drag coefficient

1. Introduction

It is well known that confining walls exert an extra retarding effect on a sphere in free fall. Knowledge of the wall effect is required if the fluid hydrodynamic drag of a sphere falling in a fluid medium of infinite extent is to be estimated. Considerable research effort has been expended in studying wall effects on a sphere falling freely in Newtonian fluids at the axis of cylindrical tubes. Consequently, a wealth of information is now available on wall effects on sphere motion in Newtonian fluids, and indeed based on a combination of numerical and experimental results, it is now possible to evaluate the wall correction factor under most conditions of practical interest, namely, the value of the sphere Reynolds number and the tube-to-sphere diameter ratios [1–4].

In contrast, little is known about the wall effects on spherical particles settling in power-law fluids. Admittedly, a substantial body of information is now available on drag on spheres in power-law fluids,

* Corresponding author. Fax: +30-1772-2251.
E-mail address: mitsouli@metal.ntua.gr (E. Mitsoulis).

0377-0257/01/$ – see front matter
PII: S0377-0257(00)00189-0

but most of such theoretical studies have not dealt with wall effects. Thus, the early studies based on the use of variational principles [5,6] assume the sphere to fall in an infinite expanse of fluid. Likewise, most numerical studies dealing with the calculation of drag on a sphere in non-Newtonian fluids [7–9] assume the far away boundary to be situated typically at 20–50 times the sphere radius, thereby minimising the contribution due to wall effects. Most of these studies have been reviewed elsewhere [10]. Caswell [11] carried out a perturbation analysis for the creeping motion of a sphere in a Rivlin–Ericksen model fluid in a cylindrical vessel and predicted the wall effects to be less severe than those in Newtonian fluids, which is consistent with early findings by Tanner [12]. The analysis on the reduction of wall effect with shear-thinning has also been reported earlier [8,12].

The assumption of the infinite expanse of fluid inherent in almost all analytical studies, however, poses a serious experimental difficulty, for such experimental studies are always carried out in fall tubes of finite size [13–15]. Another problem in the experimental studies arises from the fact that spheres will not fall along the axis and/or rotate when the sphere/tube diameter ratio exceeds ∼40%, and probably even lower in viscoelastic fluids [12]. Among the numerous workers who have reported experimental values of drag on spheres in power-law fluids, some have ignored the wall effects (e.g. [14,15]), while others [16,17] have applied the same correction as that applicable for Newtonian fluids. Neither of these procedures is generally applicable or justified. The few investigators, who have studied wall effects [8,12,13,18–20], have concluded that the wall effect is less severe in power-law fluids than in Newtonian fluids under otherwise identical conditions. This is so at least for the power-law index in the range $1 \geq n \geq 0.5$ and for sphere-to-tube diameter ratios R/R_c up to 0.5. Most of these studies have also been reviewed elsewhere [10].

From the foregoing description, it is thus, safe to conclude that few theoretical results are available on the extent of wall effects on a sphere settling in power-law fluids in cylindrical tubes even in creeping flow conditions. This work endeavours to fill this gap in the current body of knowledge on this subject. Extensive numerical results are reported herein encompassing wide ranges of conditions as $1 \geq n \geq 0$ and $0 \leq R/R_c \leq 0.5$. The latter is seen as the maximum value beyond which a sphere will fall off centre and/or rotate [12]. The paper concludes by making detailed comparisons with previous numerical simulations (for the unbounded case) and experimental results on wall effects in power-law fluids.

2. Mathematical modelling

The flow of a fluid around a sphere falling inside a cylindrical tube is shown schematically in Fig. 1. For simplicity of the calculations, it is assumed that the sphere is set and the cylinder walls are moving with the fluid velocity U. The flow is governed by the usual conservation equations for mass and momentum under isothermal conditions, i.e.

$$\nabla \cdot \boldsymbol{v} = 0, \tag{1}$$

$$\rho \boldsymbol{v} \cdot \nabla \boldsymbol{v} = -\nabla P + \nabla \cdot \boldsymbol{\tau}, \tag{2}$$

where $\boldsymbol{v}$ is the velocity vector, P the scalar pressure, $\boldsymbol{\tau}$ the extra stress tensor, and ρ the density. In Eq. (2), the inertia term has been included.

The constitutive equation that relates the non-Newtonian stresses with the velocity gradients is given by the generalised Newtonian model:

$$\boldsymbol{\tau} = \eta \dot{\boldsymbol{\gamma}}, \tag{3}$$

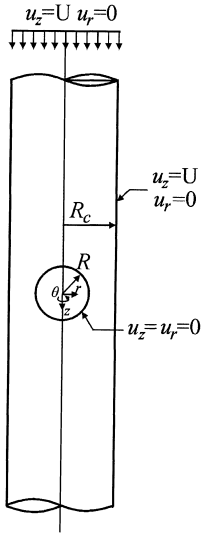

Fig. 1. Schematic representation of the falling sphere-in-a-tube geometry along with notation and boundary conditions.

where $\dot{\gamma} = \nabla \boldsymbol{v} + \nabla \boldsymbol{v}^T$ is the rate-of-strain tensor and η the non-Newtonian viscosity given by the power-law model by

$$\eta = m|\dot{\gamma}|^{n-1}, \tag{4}$$

where m is the consistency index (Pa s^n) and n the power-law index ($0 < n < 1$), while $|\dot{\gamma}|$ is the magnitude of the rate-of-strain tensor involving its second invariant.

The quantity of interest is the drag D on the sphere given by

$$D = 6\pi m \left(\frac{U}{2R}\right)^{n-1} URX(n), \tag{5}$$

where U is the sphere velocity, R the sphere radius and $X(n)$ a function of the power-law index n.

When inertia is not neglected, the generalised Reynolds number Re^* is given by

$$Re^* = \frac{\rho U^{2-n}(2R)^n}{m}. \tag{6}$$

For the flow boundary conditions and referring to Fig. 1, we impose the usual no-slip boundary condition on the sphere for the velocities, a plug profile upstream at the domain entrance and at the cylinder walls, while at the centreline we have zero radial velocity. At the exit the mass balance for the fluid is satisfied.

3. Method of solution

The governing conservation equations, Eqs. (1) and (2) together with the constitutive Eq. (3) and the appropriate boundary conditions (see Fig. 1) have been solved both by the finite-element method (FEM) and the finite-volume method (FVM) for comparison. Progressively denser types of FVM grids used

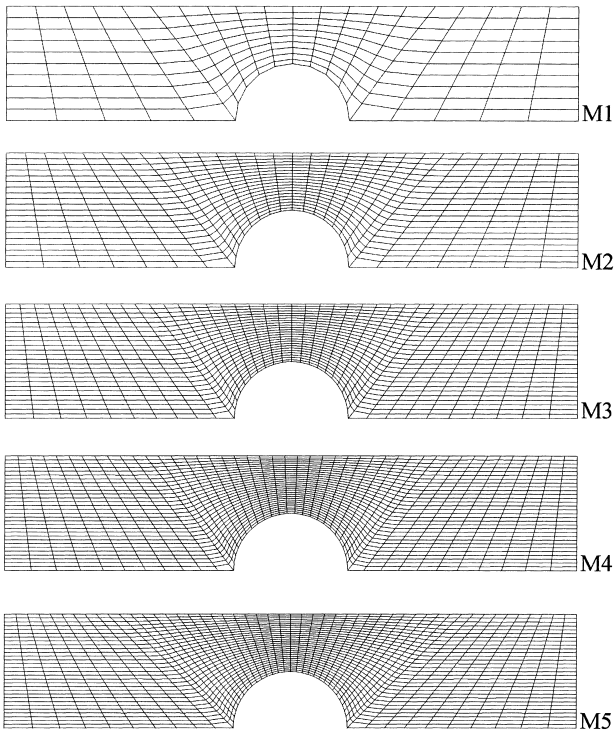

Fig. 2. Typical finite volume grids used in the computations for $R_c/R = 2{:}1$.

in the computations are shown in Fig. 2 for the geometry case of $R_c/R = 2$. Different grids have been used for different tube/sphere diameter ratios. For the FEM, the grids used have been shown in an earlier publication [21]. Tables 1 and 2 show relevant information regarding the grids used with number of control volumes, elements, and degrees of freedom, for the two different numerical methods.

Computations based on the FEM have been performed with the general FLOWCAD computer program based on the Galerkin formulation of the conservation equations for non-Newtonian fluids (e.g. [21]). Computations based on the FVM have been performed with the general FIVOS computer program [22],

Table 1
Details of the grids used with the FVM[a]

Grid	Number of cells	Number of unknowns[b]	Cell size of control volume at stagnation point	
			Symmetry line	Sphere wall
M1	200	600	2.23E−02	1.60E−02
M2	600	1800	4.39E−03	3.46E−03
M3	1000	3000	1.77E−03	1.65E−03
M4	1350	4050	1.02E−03	9.68E−04
M5	1500	4500	1.17E−03	8.01E−04

[a] Each node has six degrees of freedom. Case of $R_c/R = 2{:}1$.
[b] The number of unknowns is the number of degrees of freedom minus the number of boundary conditions.

Table 2
Details of the grids used in the FEM [21]

R_c/R	Elements	DOF
2:1	476	4286
4:1	432	3889
8:1	477	4308
10:1	423	3819
20:1	720	6504
50:1	720	6504

extended to non-orthogonal field geometry, based on a non-staggered grid arrangement, using a modified SIMPLE algorithm and the strongly implicit procedure (SIP). More details can be found in [23]. The program has been modified to handle several non-Newtonian laws according to the generalised constitutive Eq. (3).

The method of solution for the non-linear set of equations is direct substitution with continuation in the power-law index (the *n*-parameter). Solutions have been obtained down to $n = 0.1$, starting from the Newtonian solution for $n = 1$ and proceeding with reductions of 0.1. The solution process is more difficult to converge as the material becomes more shear-thinning ($n \ll 1$).

4. Results and discussion

A series of runs have been carried out with different grids and the two different methods (FEM and FVM). At a given power-law index *n*, a converged solution was considered to have been reached for the set of continuity and momentum equations when the value of all residuals was less than 5×10^{-4}. In Table 3 the total iterations needed are presented for the five grids of Fig. 2 and $n = 1.0$ (Newtonian fluid) for the case of tube/sphere diameter ratio $R_c/R = 2{:}1$. The iterations, or equivalently the computational time, exhibit a linear dependence with grid density. The execution times needed to obtain convergence for all primitive variables are presented in the same Table. Also in Table 3 is listed the calculated drag coefficient, showing the convergence of the solution to the value of 5.9474 for dense grids [21]. These results are also presented graphically in Fig. 3.

The calculations using the FVM have been performed on a PC equipped with a PENTIUM MMX-200 MHz processor. The size of the executable file was 320KB. The CPU time for $n = 0.5$ was approximately

Table 3
Calculated drag coefficient and total CPU time in seconds for computations by the FVM on a PC equipped with a Pentium processor at 200 MHz[a]

Grid	Number of iterations	Total CPU time (s)	Drag coefficient
M1	62	10	5.5822
M2	198	50	5.8546
M3	334	121	5.9223
M4	452	245	5.9447
M5	504	271	5.9471

[a] Newtonian fluid and $R_c/R = 2{:}1$.

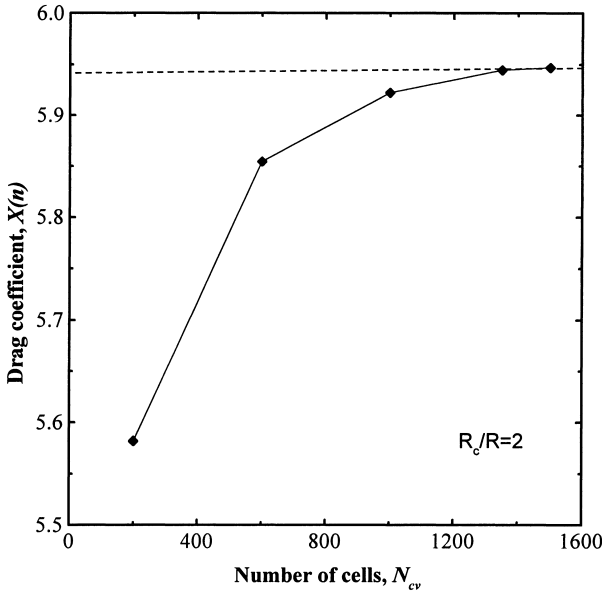

Fig. 3. Drag coefficient for flow of a Newtonian fluid around a sphere falling inside a tube for creeping flow conditions ($Re \approx 0$) and geometry ratio $R_c/R = 2{:}1$ for different grid densities (see Fig. 2).

20 min. On the other hand, the calculations with the FEM have been performed on a SGI-Power Challenge XL workstation, and the CPU time for the $n = 0.5$ was approximately 2 min.

Typical results from the simulations for the flow field (kinematics) and stress field (dynamics) are shown in Fig. 4 for the case of 2:1 diameter ratio. The results are shown as contours in terms of the two velocity components (u_r and u_z), the pressure (P) and the four stress components (normal stresses τ_{rr}, τ_{zz}, $\tau_{\theta\theta}$, and shear stress τ_{rz}). The velocities have been normalised by U, and the pressure and stresses by $m(U/R)^n$. Twenty contours have been drawn at equal intervals between the minimum and maximum values, which are shown on the graphs by open and filled circles, respectively. It is seen that due to the creeping flow conditions ($Re \approx 0$), the flow and stress fields are almost symmetric before and after the sphere, and only in the stresses there are small changes shifted in the wake of the sphere.

In Fig. 5 the drag results as a function of the power-law index n for creeping flow conditions ($Re \approx 0$) obtained from the simulations with FEM and FVM are compared for $R_c/R = 2$, 4, 8, 10, 20 and 50. These results are also listed in Table 4 for the FVM (together with quadratically extrapolated results to the unbounded case) and Table 5 for the FEM. It is seen that both FEM and FVM give almost indistinguishable results, as expected by using such dense grids. A careful examination of the numerical values shows that the FVM always gives slightly higher (at most by 0.05%) values than the FEM method, which is known to provide an upper-bound on drag, while other methods, such as the boundary element method, provide lower bounds [24]. Regarding the Newtonian case, the results when compared with the Faxen formula deviate less than 0.3% as it was the case in our previous publication [21].

As the radii ratio increases beyond 10, the differences between Newtonian and power-law behaviour become smaller, and they converge together for power-law index $n < 0.3$. The drag correction converges to a constant value in the vicinity of 1.18, independent of the tube/sphere diameter ratio, when the power-law index $n = 0$. The value of 1.18 is derived from Table 4 for $n = 0$ as the mean value of the drag

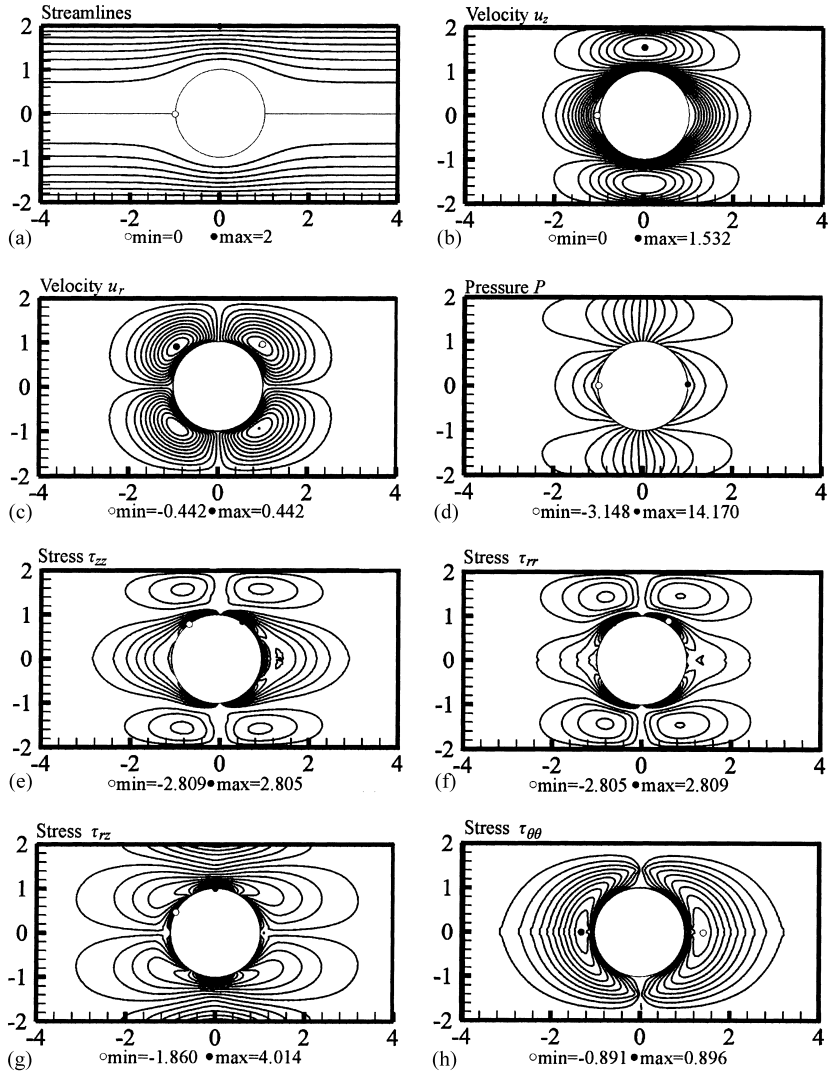

Fig. 4. (a–h) Velocity, pressure and stress fields for the case of $R_c/R = 2$:1. Power-law fluid with $n = 0.5$.

coefficient for diameter ratios $R_c/R = 2$, 4, 8, 10, 20 and 50. The standard deviation of the mean value is equal to 0.0094. It is interesting to note that the limiting value for flow of a sphere in an unbounded Bingham body at infinite Bingham number (equivalent to $n = 0$ for a power-law fluid) is 1.17, as found out by Beris et al. [25] and mentioned in our earlier publication [21].

Fig. 6 brings together results from different groups for the infinite case, approximated using quadratic extrapolation from the three cases with ratios $R_c/R = 8$, 10 and 50. In particular, the results by Wasserman and Slattery [5], Cho and Hartnett [6], and Gu and Tanner [8] are shown together with the present results. The differences are due to the fact that the works by Wasserman and Slattery [5], and Cho and Hartnett [6] are based on an upper-bound found by variational principles, while the work by Gu and Tanner [8] is

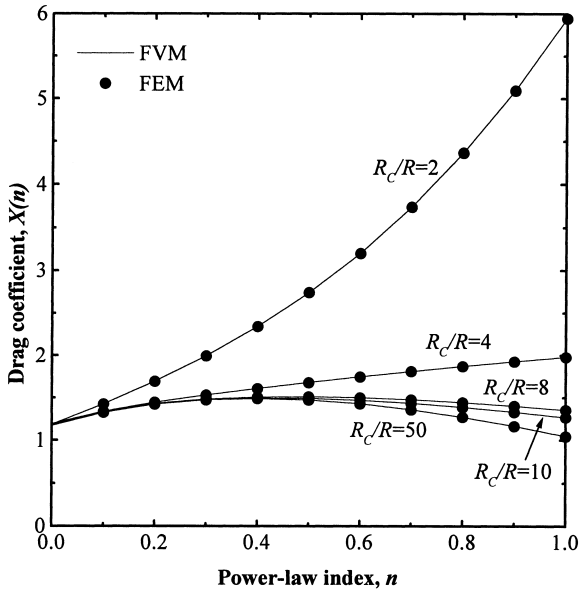

Fig. 5. Drag coefficient for flow around a sphere falling inside a tube for creeping flow conditions ($Re \approx 0$) and geometry ratios $R_c/R = 2, 4, 8, 10, 20$ and 50 for both FVM and FEM methods. The fluid is assumed to be shear-thinning obeying the power-law model (Eq. (4)).

based on similar FEM results using rather sparse grids. Therefore, our results offer an improvement over all previous findings for this case.

As mentioned previously, Chhabra and Uhlherr [20] reported extensive results on wall effects on sphere motion in a series of power-law fluids. The material properties for three of these fluids are given in Table 6. They measured the terminal settling velocity of numerous spheres in up to 10 cylindrical tubes (of different diameters) filled with power-law fluids. The corresponding unbounded medium terminal

Table 4
The values of the drag correction factor *X(n)* from the FVM simulations for different R_c/R ratios

n	2	4	8	10	20	50	∞
1.0	5.9471	1.9806	1.3551	1.2672	1.1194	1.0464	1.0055[a]
0.9	5.0957	1.9262	1.4030	1.3307	1.2146	1.1636	1.1371[a]
0.8	4.3686	1.8696	1.4439	1.3873	1.3014	1.2700	1.2558[a]
0.7	3.7422	1.8096	1.4774	1.4347	1.3767	1.3595	1.3554[a]
0.6	3.2021	1.7461	1.4995	1.4695	1.4360	1.4291	1.4322[a]
0.5	2.7411	1.6791	1.5108	1.4923	1.4754	1.4738	1.4787[a]
0.4	2.3414	1.6075	1.5077	1.4959	1.4900	1.4908	1.4973[a]
0.3	1.9953	1.5321	1.4850	1.4760	1.4752	1.4767	1.4839[a]
0.2	1.6931	1.4465	1.4331	1.4232	1.4233	1.4250	1.4334[a]
0.1	1.4267	1.3387	1.3361	1.3268	1.3269	1.3300	1.3386[a]
0.0	1.1847[a]	1.1934[a]	1.1718[a]	1.1708[a]	1.1723[a]	1.1818[a]	1.1834[a]

[a] By extrapolation.

Table 5
The values of the drag correction factor $X(n)$ from the FEM simulations for different R_c/R ratios

n	2	4	8	10	20	50	∞
1.0	5.9441	1.9796	1.3544	1.2666	1.1190	1.0459	1.0035[a]
0.9	5.0931	1.9253	1.4023	1.3300	1.2140	1.1630	1.1367[a]
0.8	4.3664	1.8686	1.4431	1.3866	1.3007	1.2693	1.2568[a]
0.7	3.7403	1.8087	1.4767	1.4340	1.3761	1.3589	1.3546[a]
0.6	3.2005	1.7452	1.4988	1.4688	1.4353	1.4284	1.4293[a]
0.5	2.7397	1.6783	1.5100	1.4916	1.4746	1.4730	1.4755[a]
0.4	2.3402	1.6067	1.5070	1.4952	1.4893	1.4901	1.4924[a]
0.3	1.9943	1.5313	1.4843	1.4752	1.4744	1.4759	1.4778[a]
0.2	1.6923	1.4457	1.4324	1.4225	1.4226	1.4243	1.4261[a]
0.1	1.4260	1.3380	1.3354	1.3261	1.3262	1.3293	1.3327[a]
0.0	1.1841[a]	1.1928[a]	1.1712[a]	1.1702[a]	1.1771[a]	1.1812[a]	1.1840[a]

[a] By extrapolation.

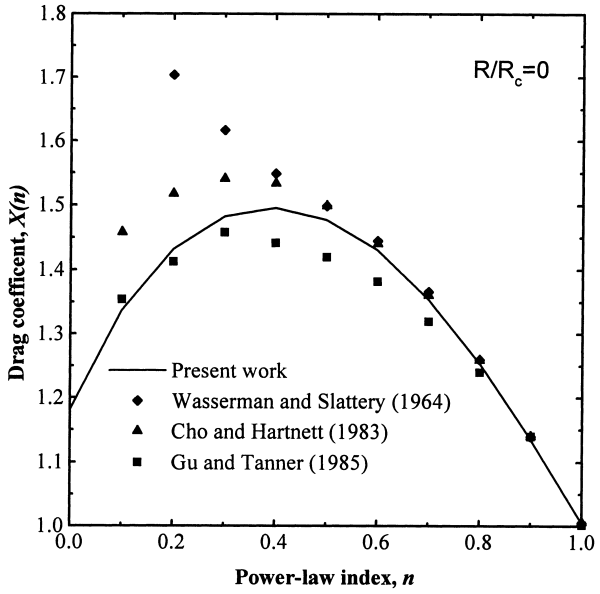

Fig. 6. Drag coefficient for flow around a sphere falling inside a tube for creeping flow conditions ($Re \approx 0$). Present results extrapolated for the unbounded case in comparison with theoretical and computational results from other research groups.

Table 6
Power-law parameters for the test fluids

Test fluid	Temperature T (°C)	Density ρ (kg/m^3)	Consistency index m (kPa s^n)	Power-law index n
V2	20.0	1000	0.095	0.90
V4	18.8	1000	0.082	0.86
V8	20.0	1000	0.340	0.67

velocity U_∞ of each sphere was evaluated by plotting the measured terminal velocity U versus R/R_c, and then extrapolating these linear plots to $R/R_c = 0$ thereby yielding the value of U_∞. This, in turn, allows the wall correction factor, f, to be defined as

$$f = \frac{U}{U_\infty}. \tag{7}$$

Evidently, f takes on values between 0 and 1. Based on a detailed analysis of their experimental data and by analogy with the behaviour observed in Newtonian fluids, the wall correction factor, f, was found to be independent of the sphere Reynolds number up to about 1, i.e. in the creeping flow regime. Furthermore, the power-law index also was found to be an insignificant variable at 90% confidence level, at least in the range of experimental conditions ($1 \geq n \geq 0.5$). Chhabra and Uhlherr [20] proposed the following empirical correlation for f:

$$f = 1 - 1.6\left(\frac{R}{R_c}\right). \tag{8}$$

It is thus, appropriate to contrast the present numerical predictions with that of Eq. (8). It can easily be shown that for a power-law fluid, the wall correction factor f is related to the drag correction factor $X(n)$ through the following simple expression:

$$f = \left(\frac{X_\infty}{X}\right)^{1/n}, \tag{9}$$

where X_∞ corresponds to the unbounded case (values reported in Table 4) and X relates to a specific value of R_c/R, also listed in Table 4.

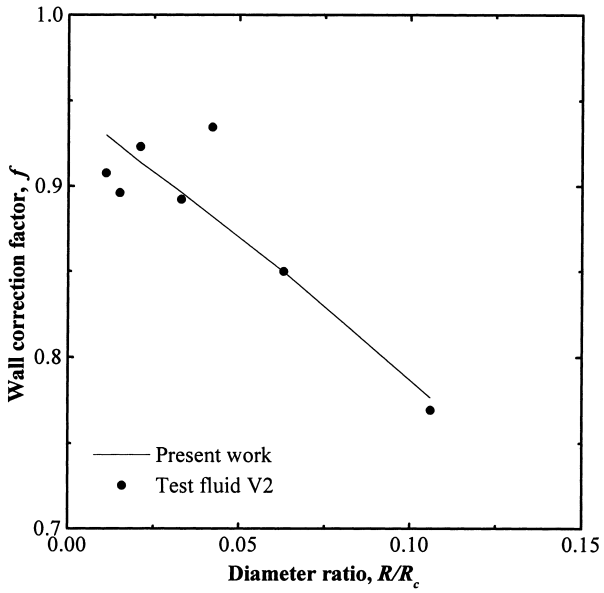

Fig. 7. Wall correction factor for flow around a sphere falling inside a tube for creeping flow conditions ($Re \approx 0$) and different R/R_c ratios. Present computational results in comparison with experimental results for test fluid V2.

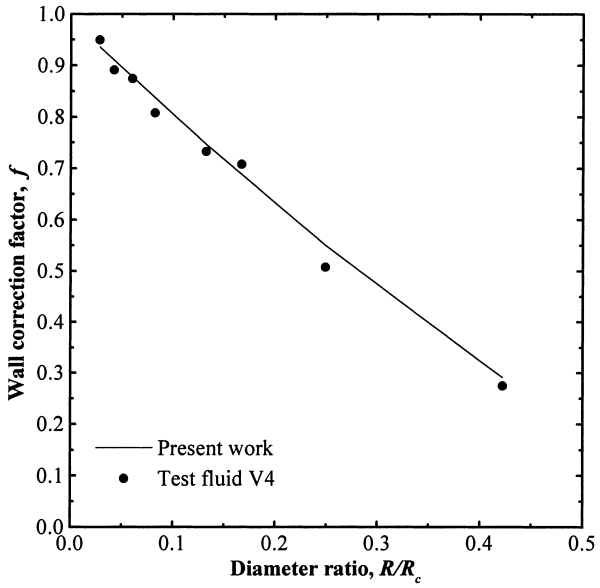

Fig. 8. Wall correction factor for flow around a sphere falling inside a tube for creeping flow conditions ($Re \approx 0$) and different R/R_c ratios. Present computational results in comparison with experimental results for test fluid V4.

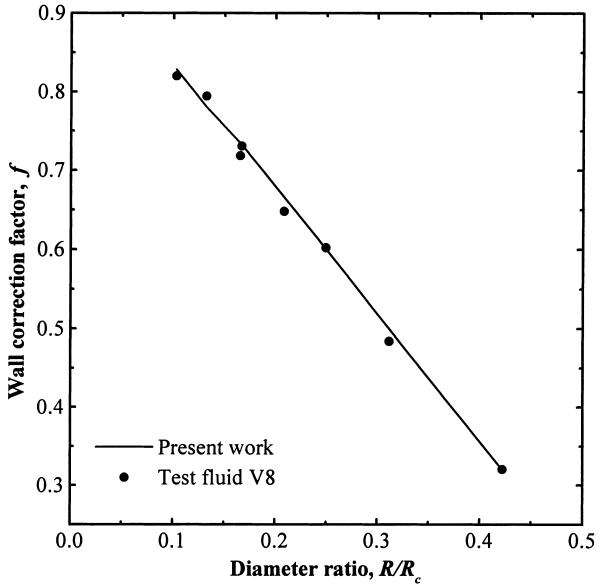

Fig. 9. Wall correction factor for flow around a sphere falling inside a tube for creeping flow conditions ($Re \approx 0$) and different R/R_c ratios. Present computational results in comparison with experimental results for test fluid V8.

Figs. 7–9 contrast the present numerical results with the experimental results of Chhabra and Uhlherr [20] for the perspex spheres settling in three of their test fluids over a range of values of R/R_c. An examination of these figures shows excellent match between predictions and experimental data up to about $R/R_c = 0.43$. A similar sort of correspondence is observed for other test fluids and hence the results are not shown here. Suffice it to add that while the experimental results, approximated here by Eq. (8), suggest the power-law index not to be a significant variable, the numerical simulations suggest that for a constant value of R/R_c the value of f rises with decreasing value of n, thereby further reaffirming that the wall effects diminish with increasing degree of pseudoplasticity. This finding is consistent with the analysis of Caswell [11]. Finally, it is worthwhile to add that the present numerical simulations and the predictions of Eq. (8) progressively diverge with increasing values of R/R_c and/or with decreasing values of n.

5. Conclusions

The flow around a sphere falling inside tubes filled with shear-thinning fluids obeying the power-law model, has been simulated by both the FEM and the FVM with similar results. The methods are comparable in these kinds of problems in computational speed, but the FEM requires more space.

The numerical results are in very good agreement with previous experimental results. New results for the drag around a sphere show that the tube/sphere diameter ratio has a strong influence on the drag, showing an increase and then a decrease as the shear-thinning character of the fluid increases (lower power-law index n).

The present work has revealed that when the power-law index n approaches zero, the drag coefficient converges to a constant value of 1.18, which is independent of the tube/sphere diameter ratio.

The present results can be used for deducing the rheological parameters m and n of the model in such experiments with polymer solutions, which are easy and fast to do in the laboratory. This is done by knowing the diameter ratio and measuring the drag, and then from the present results finding out the value of n. Two different measurements can be used to deduce the value of m.

References

[1] J. Happel, H. Brenner, Low Reynolds Number Hydrodynamics, Prentice Hall, NJ, 1965.
[2] R. Clift, J. Grace, M.E. Weber, Bubbles, Drops and Particles, Academic Press, New York, 1978.
[3] P.H.T. Uhlherr, R.P. Chhabra, Can. J. Chem. Eng. 73 (1995) 918–923.
[4] R.M. Wham, O.A. Basaran, C.H. Byers, Ind. Eng. Chem. Res. 35 (1996) 864–873.
[5] M.L. Wasserman, J.C. Slattery, AIChE J. 10 (1964) 383–394.
[6] Y.I. Cho, J.P. Hartnett, J. Non-Newtonian Fluid Mech. 12 (1983) 243–247.
[7] K. Adachi, N. Yoshioka, K. Sakai, J. Non-Newtonian Fluid Mech. 3 (1977/1978) 107–125.
[8] Gu Dazhi, R.I. Tanner, J. Non-Newtonian Fluid Mech. 17 (1985) 1–12.
[9] M.B. Bush, N. Phan-Thien, J. Non-Newtonian Fluid Mech. 16 (1984) 303–313.
[10] R.P. Chhabra, Bubbles, Drops and Particles in Non-Newtonian Fluids, CRC Press, Boca Raton, 1993.
[11] B. Caswell, Chem. Eng. Sci. 25 (1970) 1167–1176.
[12] R.I. Tanner, Chem. Eng. Sci. 19 (1964) 349.
[13] T. Sato, I. Taniyama, S. Shimokawa, Kagaku-Kogaku 4 (1966) 215–219.
[14] B. Mena, B. Caswell, Chem. Eng. J. 8 (1974) 125–139.
[15] A. Acharya, R.A. Mashelkar, J. Ulbrecht, Rheol. Acta 15 (1976) 454–470.

[16] H. Kato, M. Tachibana, K. Oikawa, Bull. JSME 15 (1972) 1556.
[17] D. Sigli, M. Coutanceau, J. Non-Newtonian Fluid Mech. 2 (1977) 1–21.
[18] R.M. Turian, AIChE J. 13 (1967) 999–1006.
[19] P.H.T. Uhlherr, T.N. Le, C. Tiu, Can. J. Chem. Eng. 54 (1976) 497–502.
[20] R.P. Chhabra, P.H.T. Uhlherr, Chem. Eng. Commun. 5 (1980) 115–122.
[21] J. Blackery, E. Mitsoulis, J. Non-Newtonian Fluid Mech. 70 (1997) 59–77.
[22] K.A. Missirlis, FIVOS: A FInite Volume Solver for Non-Newtonian Flows, Internal Report, Department of Chemical Engineering, NTUA, Athens, Greece, 1996.
[23] K.A. Missirlis, D. Assimacopoulos, E. Mitsoulis, J. Non-Newtonian Fluid Mech. 78 (1998) 91–118.
[24] R.I. Tanner, J. Non-Newtonian Fluid Mech. 38 (1990) 101–106.
[25] A.N. Beris, J.A. Tsamopoulos, R.C. Armstrong, R.A. Brown, J. Fluid Mech. 158 (1985) 219–244.